Journal Title
XX(X):2–34

DOI: 10.1177/ToBeAssigned
www.sagepub.com/
SAGE

Damage detection, quantification and localization for resonant metamaterials using physics-based and data-driven methods

Y.C. Zhu [1], S. Cantero-Chinchilla [2], H. Meng [3], W.J. Yan [4] and D. Chronopoulos [5]

Abstract

Resonant metamaterials have attracted significant research interest in mechanical and acoustic engineering with applications in the fields of sound and vibration control thanks to their integrated tuned mass dampers. One prevailing issue regarding industrial application of such structures is the high probability of local damage for their resonating parts. Accurate and efficient health state estimation methods for resonant metamaterials are therefore urgently required. In particular, the quantification and localization of damaged resonators represent key pieces of information for the operator of a structural asset. This work presents for the first time an investigation into quantifying and identifying damaged oscillators in a resonant metamaterial based on the measured frequency response function data. Both data-driven and physics-based methods are implemented and corresponding results are exhibited. Manufacturing-induced structural uncertainty is quantified through physical measurements and taken into account in this work. It is demonstrated that such uncertainty may have a rather significant impact on the response of 3D printed resonant metamaterials, leading to difficulties vis-a-vis damage quantification. The proposed theoretical developments are able to properly account for such uncertainties, providing probabilistic estimation indices for the existing damage level and location. Both simulated and experimental case studies are presented to validate the two proposed methodologies and comparisons are also exhibited and discussed.

Keywords

Metamaterials, Resonators, Vibration, Structural Health Monitoring, Damage Identification and Quantification

Introduction

Optimally designed metamaterials can manipulate electromagnetic, elastic and acoustic waves in a human-defined manner not observed in bulk materials. Those families of metamaterials exhibiting a negative index of refraction for particular wavelengths have attracted significant research over the last twenty years, with several potential applications being envisaged including cloaking [1], filters for medical imaging [2], remote space applications, ultrasound signal filters for infrastructure monitoring [3], smart solar power management, crowd control, high-frequency communication and lenses for high-gain antennas [4], attenuating noise and vibration and even shielding structures from earthquakes [5]. With specific regard to mechanical and acoustic wave manipulation [6], locally resonant metastructures are finite structures exploiting locally resonant metamaterial concepts for low-frequency vibration attenuation as a result of stop band formation for wavelengths much larger than the lattice periodicity. Such structures have phenomenologically increased impedance (thus reduced vibration levels) within their stop band regions thanks to energy absorption and dissipation through their integrated tuned mass-damper resonators. A prevailing issue vis-a-vis the applicability of such metastructures within industrial systems is the high probability of local failure due to the number of intensely resonating parts. It should be noted that increasing the thickness of the resonant parts would ruin optimality and performance of the design and therefore constitutes no option for engineers. There is consequently a compelling need for accurately and efficiently extracting as much health state information as possible for such metastructures. Such information should not only be limited to damage detection (since a single breakage would not be structurally critical, thus probably tolerable), but should ideally quantify the number of damaged resonators and their locations within the metastructure.

Generally, structural damage detection can be classified as local-damage detection and global-damage detection [7]. The former refers to non-destructive testing such as ultrasonic guided wave, acoustic emission and electromagnetic testing, etc., which are

[1] Department of Bridge Engineering, School of Transportation, Southeast University, Nanjing, China
[2] Department of Mechanical Engineering, University of Bristol, Bristol, BS8 1TR, UK
[3] Department of Mechanical and Construction Engineering, Northumbria University, NE1 8ST, United Kingdom
[4] State Key Laboratory of Internet of Things for Smart City and Department of Civil and Environmental Engineering, University of Macau, China
[5] Department of Mechanical Engineering & Mecha(tro)nic System Dynamics (LMSD), KU Leuven, 9000, Belgium

Corresponding author:
Yi-Chen Zhu
Email: zhuyichen@seu.edu.cn

mainly used to evaluate the local properties of a structure for characteristic differences or defects. Baseline data of the healthy structure are not always necessary since these approaches can employ baseline data extracted from the damaged structure [8, 9]. However, this local damage detection methodology can only be used to detect some special components of a structure [10, 11]. In order to be able to inspect the entire structure (especially regarding complicated structures), researchers have developed global approaches based on the measurements of vibration signals over the last three decades [12, 13]. The rationale of global damage detection approaches is that damage changes the stiffness of the structure and therefore the behavior of vibration-based index such as natural frequencies [14], mode shapes [15], modal strain energy [16], modal flexibility [17], frequency response function (FRF) [18] and transmissibility [19], which can be obtained from the results of dynamic testing. Among others, FRF to be used in this study has been widely recognized as an appropriate approach to quantify the health state of an inspected structure. Sampaio and Maia [20] proposed a damage indicator, the FRF curvature, to locate and quantify the damage. Motivated by the concept of the modal assurance criterion (MAC), a response vector assurance criterion (RVAC) was proposed in [20] for damage detection by considering the correlations of the FRFs. The rationale behind RVAC is that less correlation indicates greater damage. Esfandiari [21, 22, 23] investigated the sensitivity-based model updating technology based on FRF, which was then applied to locate and quantify damage of beams. Recently, FRF-based damage detection was conducted within the Bayesian framework by accommodating multiple sources of uncertainty in [24].

According to [25], the damage identification problem can also be addressed using an inverse problem where a high-fidelity physical model of the structure is required [26] or as a pattern recognition problem requiring a statistical model representation of the system [27]. For the model-based approach, the concept of damage sensitivity equations [28] is usually used in an inverse problem which can be based on any type of data, e.g. modal data or time series. The resulting inverse problem usually is ill-posed, and therefore special attention such as $l1$ regularization [29] or sparse regularization [30] are usually required for an accurate solution. The deterministic approaches are more likely to produce poor results in practice. Therefore, the problem of how to treat the uncertainties explicitly always arises [31, 32]. One novel research stream is the Bayesian approach which is able to find the plausible structural damage extents as well as their probabilities given a model of the structural system and the measured data [33, 34].

Different from the inverse-problem approaches, a data-based strategy for structural health monitoring (SHM) is based on the idea that measured data from the system of interest are assigned a damage class by a pattern recognition algorithm [25]. The data-based approaches usually make extensive use of statistical models rather than the physics-based ones. One extracts damage-sensitive features from the measurements, which are then combined with a machine learning analysis to construct statistical models of the different classes one wishes to distinguish and a classifier to determine which class new data might belong to. There are two main types of learning in

the context of vibration-based SHM: supervised learning and unsupervised learning [25, 35]. Supervised learning algorithms learn to associate labels with features from the training data which consist of a set of feature vectors together with their known class labels, while unsupervised algorithms are usually applied in a two-class problem where feature data are only known for one class [36]. The damage detection level can be realized by unsupervised learning algorithms which only requires data from the normal condition of the structure [37]. However, damage localization ought to be achieved by dividing the structure into substructures and assigning a class label for data corresponding to damage in given substructures. One may need data from the structure of interest in many different damage scenarios which may be impossible or at least very expensive to obtain. Similarly, the damage assessment level requires data for different damage extents with each dataset represented by a class label for the classifier [25]. Therefore, the availability of damage state data is a serious issue for data-driven SHM.

We hereby report for the first time an investigation into quantifying and identifying defects in resonant metamaterials. Specifically, this work focuses on breakage of the integrated resonators. Major novelty of this work includes:

1. A hierarchical Bayesian framework is developed to rigorously estimate three levels of damage-related information in resonant metamaterials with quantified uncertainty: (1) the number of broken resonators, (2) their locations within the beam structure, and (3) updated model parameters.
2. Damage indices are proposed to account for the manufacturing-induced structural uncertainty. A data-driven scheme is then employed based on the proposed damage indices to assess the level of damage (number of broken resonators) in the metastructure.
3. Both numerical and experimental case studies involving populations of damaged metamaterial beam structures are exhibited to validate the developed quantification and identification methodologies.

The manuscript is organised as follows. The details of the resonant metamaterials investigated in this work are first presented as well as the measurement configurations for obtaining FRF data. Comparison between the measured FRFs and the theoretical predictions are discussed, illustrating the uncertainties encountered. To eliminate the effect of experimental uncertainty, damage indices are then proposed. The main theory of both physics-based and data-driven methods used in this work are reviewed. Numerical and experimental data are presented to validate the developed methods.

The Resonant Metamaterial under Investigation

In this work, the FRFs of the resonant metamaterials are measured for damage identification and quantification. Specifications of the experimental samples tested in this work as well as the instrumentation details are presented in this section. The measured FRFs of the experimental samples are then compared with the theoretical model predictions, illustrating the uncertainties involved in manufacturing process.

Experimental testing procedure

The considered metamaterial beam is composed of Π-shaped backbone with parallel insertions and attached cantilever-mass resonators as shown in Figure 1. It's experimental realisation can be found in Figure 2a. The metamaterial beam can exhibit single or multiple bandgaps depending on whether the two sets of resonators attached to different side walls are symmetric. In this work, asymmetric resonators are considered.

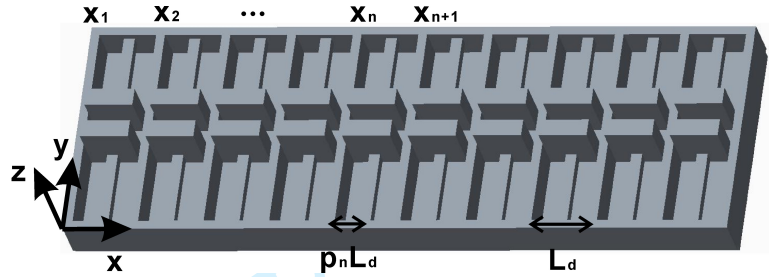

Figure 1. Schema of the metamaterial beam with cantilever-mass resonators

In order to investigate the FRFs of the metamaterial beam, 12 beams were manufactured with Nylon-12 powder by Selective Laser Sintering method, which is one of the most popular additive manufacturing methods. The Nylon 12 powder was filled in a powder bed, then sintered layer by layer to the designed shapes with a laser. The printed structures have a density ρ of 948.9 kg/m^3, a flexural modulus E_0 of 1.62 GPa and a loss factor η of 0.01. The geometric parameters of the beams are listed in Table 1.

Table 1. Geometrical parameters of tested metamaterial beams

Backbone	
Height	H_d=10 mm
Width	w_d=49 mm
Side wall thickness	t_d=2 mm
Backplate thickness	b_d=4 mm
Insertions	
Plate insertion thickness	t_w=10 mm
Distance between plate insertions	L_d=15 mm
Number of segments	q=10
Resonators	
Height of cantilever beam	h_{s1}=2.4 mm,h_{s2}=2.3 mm
Width of cantilever beam	b_{s1}=2.5 mm,b_{s2}=2.4 mm
Length of cantilever beam	l_{s1}=l_{s2}=19.5 mm
Resonator mass	m_{r1}=m_{r2}=0.55 g

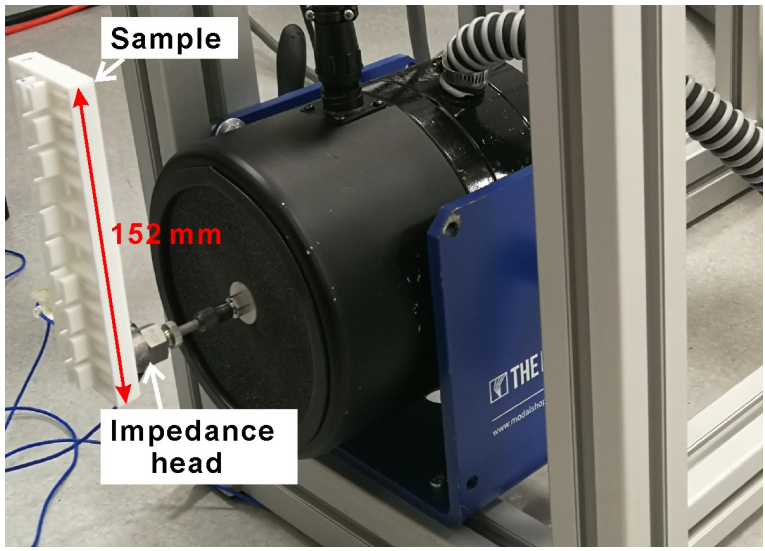

(a)

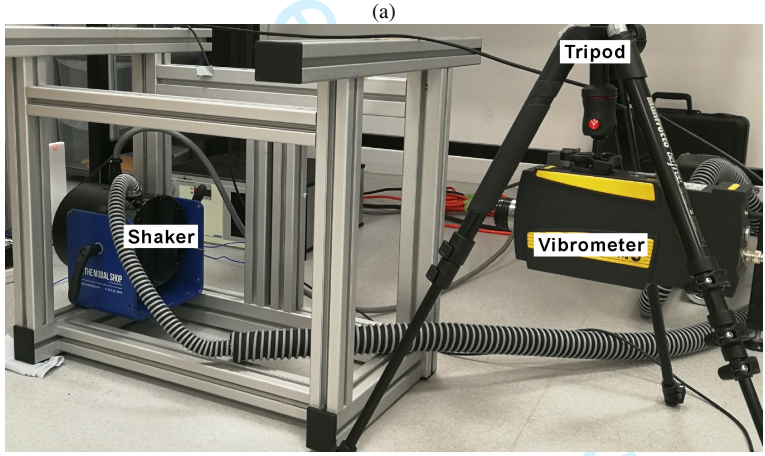

(b)

Figure 2. Photos of the tested metamaterial beam and experimental setup for the receptance test: (a) partial view, (b) global view

The receptance functions of beams were tested by an experiment system as shown in Figure 2a and 2b. The measurement system is composed of a Doppler laser vibrometer (Polytec PDV-100), a mechanical shaker (Modal Shop 2060E), an impedance head (PCB 288D01) and auxiliary components. The samples are glued firmly to the impedance head which is screwed to the mechanical shaker at the other end. A chirp signal source that is generated by the computer and then amplified by an amplifier determines the output forces by the mechanical shaker. The impedance head measures the actual excitation

forces on the metamaterial beam. Displacements at the other end of the beam are measured by the laser vibrometer. The receptance functions can be derived by the ratios between the tested displacements and excitation forces.

Comparison between experimental and analytical results

The FRFs of the metamaterial beam can be calculated analytically by the displacement transfer matrix model [38, 39, 40]. The receptance functions of metamaterial beams calculated by the analytical model are compared with that measured experimentally as shown in Figure 3. Discrepancies can be found between the theoretical model predictions and experimental measurements. Differences between the two curves mainly lie in the resonance frequency of the beam, which are mainly due to the manufacturing uncertainties, simplifications in the analytical model and non-ideal experimental conditions. Especially, it has been found that uncertainties of physical parameters and geometric dimensions from manufacturing process can affect the FRFs of the metamaterial beam dramatically [40]. Such uncertainties also lead to calibration issues when applying the physics-based damage identification and quantification method to experimental data. Detailed analysis can be found in the next section.

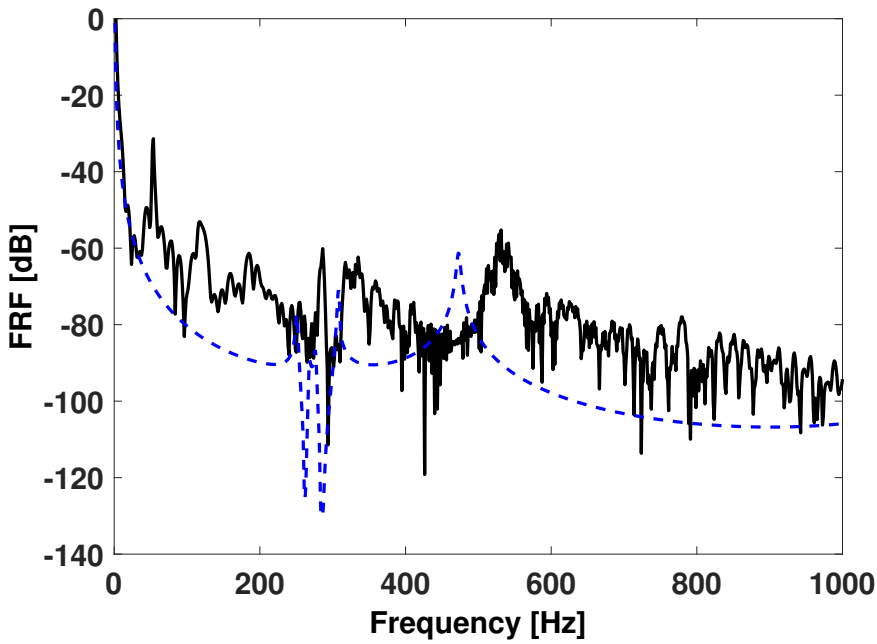

Figure 3. Comparison of receptance functions by analytical evaluation and experimental measurement. (Solid line: experimental; dashed line: analytical)

Damage Features and Indices

The properties of FRFs with damaged resonators are investigated and the feasibility of applying data driven damage quantification methods are discussed in this section. Due to the nature of resonant metamaterials as well as the involved uncertainties induced through manufacturing and measurement procedures, conducting damage quantification directly based on FRFs can be quite challenging. In view of this, damage features are investigated and damage index extraction strategy is proposed in this section to overcome these issues.

Properties of FRFs with broken resonators

In order to choose proper damage identification and quantification features for the metamaterial beam, the properties of its FRFs with different numbers and locations of broken resonators are investigated in this section. Figure 4 shows the numerical predictions of FRFs based on the theoretical models with sequence of missing resonators (randomly picked). Differences can be found in the FRFs with different numbers of missing resonators, illustrating the feasibility of conducting damage identification and quantification based on FRF data. However, challenging issues are still encountered when applying data-driven models directly on the FRF data, which are listed as follows.

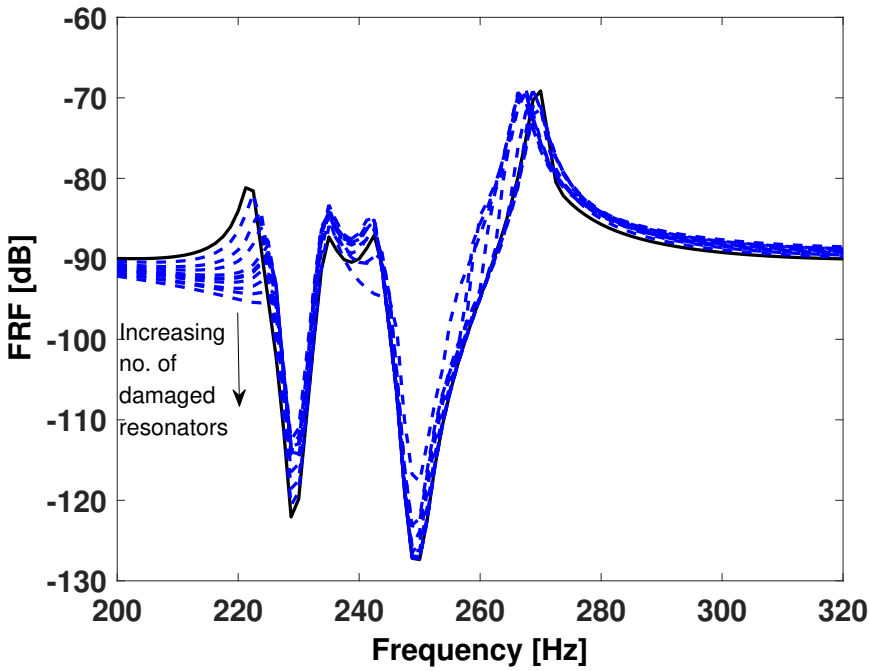

Figure 4. Numerical predictions of FRFs with broken resonators (Solid line: undamaged; dashed line: damaged)

- Dimension of the input features will be very high when directly applying FRFs data to data-driven models. The resulting damage identification and quantification method will lack computation efficiency. Dimension reduction techniques can be applied as pre-process steps (e.g., Principal Component Analysis [41]) but the resulting features are obtained in a fully data-driven manner without direct physical interpretation. Noting that there are also discrepancies between the FRFs of experimental data and theoretical model predictions. This will cause problems in applying outcomes from the data-driven space to the physics-driven one and vice-versa.
- Even when the number of missing resonators is the same, FRFs of the metamaterial beams can behave quite differently. It is also possible that the FRFs are close when for two damage cases with different number and locations of missing resonators. Figure 5 shows a typical example of such situation. The dashed line and the dashed line with dots represent two samples with one broken resonator, which are not close. The former is much closer to the undamaged case (the solid line). This relatively simple example illustrates the issues encountered when inferring the number of broken resonators in the metamaterial beam.

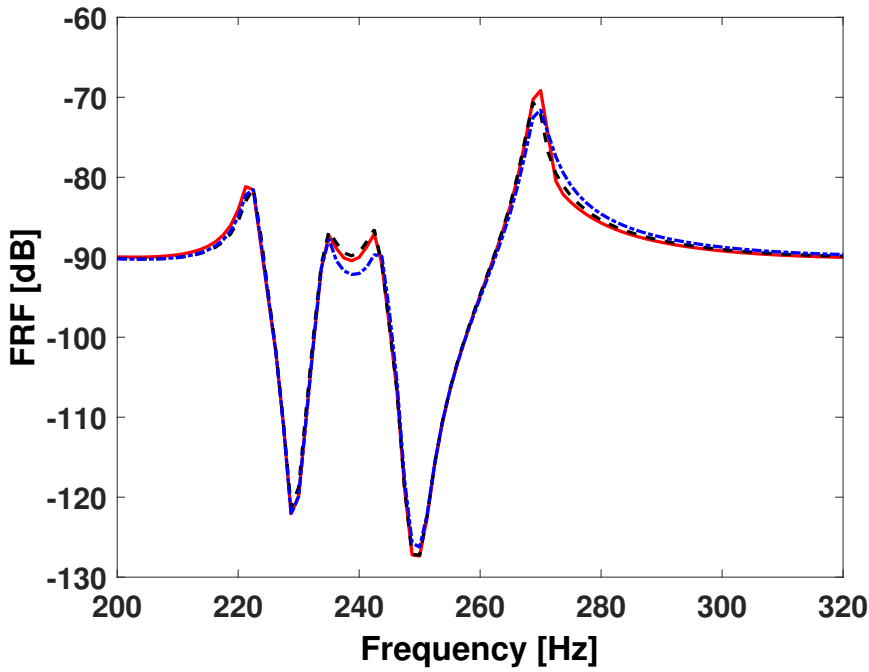

Figure 5. A typical example of FRF under different damage situation (Solid line: undamaged; dashed line: resonator no.15 damaged; dashed line with dots: resonator no.5 damaged)

One way to overcome the foregoing issues is to first extract damage features from FRF data that are sensitive to the number of broken resonators. Significant changes can be found around the spectral peak and through of FRFs within the frequency bands of [210,225] Hz and [240, 255] Hz, respectively. Two damage features are hence considered, i.e., the integral of FRFs within these two frequency bands, respectively. Numerical investigation has been conducted to assess these two damage features. One hundred numerical metamaterial samples have been simulated with the number of missing resonators ranging from 1 to 10. The locations of missing resonators are randomly selected for each sample. Figure 6 shows the first two PCAs of these samples based on the FRF data and Figure 7a shows the selected damage features of these samples. It can be seen that compared to the first two principal components obtained using PCA, the extracted damage features provide similar performance where the samples within different number of broken resonators are gathered in groups. This indicates that the selected features extract the damage information from the FRF properly, providing opportunities of later applying clustering approaches for damage quantification. Compared to PCAs that are fully data-driven, the proposed damage indices can provide similar performance but with more insightful interpretation towards the physical properties of the metamaterials (i.e., the location of spectral peaks). This is beneficial when applying them from numerical simulation to experimental samples where the location of spectral peaks may be different.

Damage index extraction strategy

Analysis in the last section demonstrates the feasibility of conducting damage quantification based on the extracted damage features. The extraction strategy is hereby further investigated. The numerical simulation discussed above does not involve uncertainties. The standard deviation of density and Young's modulus of the metamaterials resulting from the manufacturing process are presented in the appendix and the induced impact on the measured FRFs is quite significant. Figure 7b shows the simulation results where such material uncertainties are taken into consideration. It can be seen the resulting realisation based on the current damage features is rather fluctuating and it is not possible to cluster the data in clearly distinguished classes. In view of this, damage indices that could eliminate the material uncertainties and the discrepancies between different tested metamaterials would be preferred. Considering that the spectral peaks in FRFs also vary with material properties, the frequency band for extracting damage features should be determined in a relative way, i.e., based on the location of spectral peaks for each sample of the population, rather than fixed deterministic values. Noting that the FRF of the healthy structure are a priori known, the damage indices can be further normalised with respect the damage index values under health condition to further eliminate the effect due to variations between samples of the population.

Eventually, damage index 1 is obtained as follows. The location of the first spectral peak in the FRF of the sample under investigation is firstly localized. Then the lower and upper bound of the frequency band is set as $\pm$5Hz of the resonance frequency. Then the integral of the FRF is calculated within the frequency range of interest and the value is set

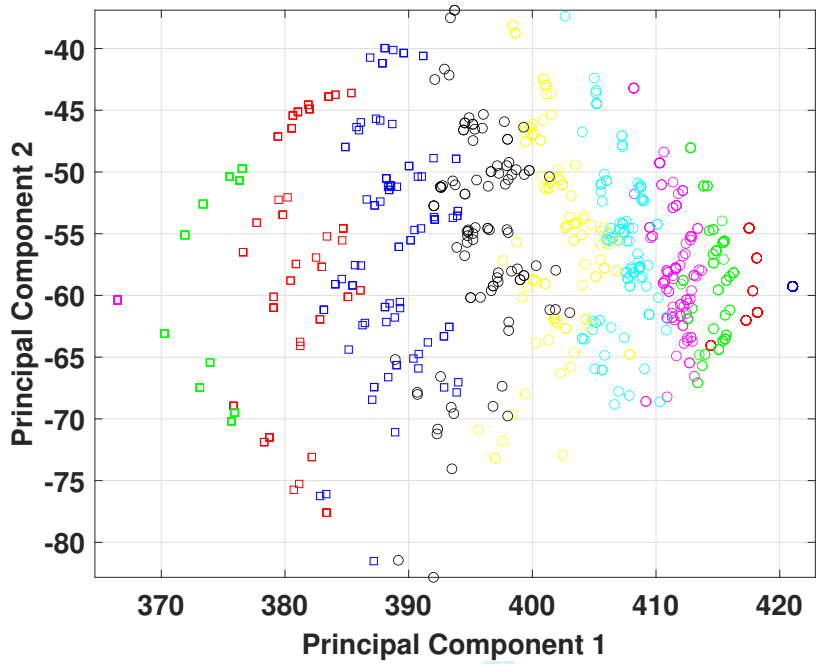

Figure 6. Observation of simulated data based on PCA (No. of damaged resonators, blue circle: 0; red circle: 1; green circle: 2; magenta circle: 3; cyan circle: 4; yellow circle: 5; black circle: 6; blue square: 7; red square: 8; green square: 9; magenta square: 10)

as a reference one, namely $F_{\text{undamaged}}$. For this sample structure under a certain damage condition, the integral of FRFs within the frequency band is calculated, namely F_{damaged}. The Damage Index 1 is then calculated as:

$$\text{Normalised Damage Index 1} = \frac{(F_{\text{damaged}} - F_{\text{undamaged}})}{\text{abs}(F_{\text{undamaged}})} \tag{1}$$

Following a similar procedure, the second damage index is calculated based on the integral of FRFs within $\pm$5Hz of the lowest point in the recorded FRF. Figure 8 shows the realisations of simulated data with uncertainty involved based on the proposed 'normalised' damage indices. It can be seen that the distributions of the sampled data are similar to the case when there is no uncertainty involved (as initially shown in Figure 7a), indicating that the proposed damage indices are capable of eliminating the effect of material uncertainties and discrepancies among the population.

Having said that, quantifying the number of broken resonators is rather challenging. Data with different numbers of broken resonators are still overlaid based on the proposed normalised damage indices. Instead of applying hard clustering methods, it would be

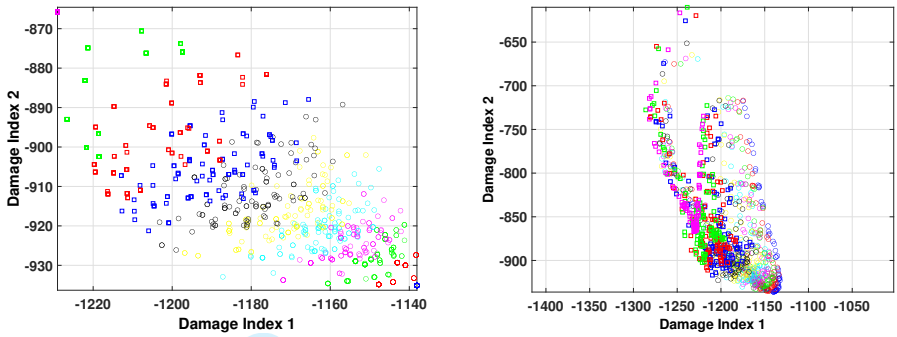

(a) without uncertainty **(b)** with material uncertainty

Figure 7. Observation of simulated data based on damage indices (No. of damaged resonators, blue circle: 0; red circle: 1; green circle: 2; magenta circle: 3; cyan circle: 4; yellow circle: 5; black circle: 6; blue square: 7; red square: 8; green square: 9; magenta square: 10)

more appropriate to conduct flexible clustering on data, that is assessing the probability of a data point being part of a cluster.

It should also be noted that the bandwidth of the FRFs used for damage index extraction is not fixed (e.g., $\pm$5Hz of the resonance frequency in this work). A wider frequency band can include more damage information but will increase the data dimension and involve more modelling error. On the other hand, a narrow frequency band can increase computation efficiency but will lose information. In applications, a proper frequency band should be set balancing computational efficiency and damage quantification quality.

Damage Identification and Quantification Methods

Both physics-based as well as data-driven methods are applied in this work for conducting identification and quantification of damage in resonant metamaterials. A physics-based multi-level Bayesian inverse method is applied to explore the possibility of identifying the location of damaged resonators. On the other hand, a data-driven method is applied to quantify the number of damaged resonators where the training data for each damage class is assumed to be Gaussian distributed. The theoretical background of these two methodologies are reviewed in this section.

Physics-based approach: A multi-level Bayesian inverse method

Damage quantification and identification is simultaneously addressed using a multilevel Bayesian approach based on [42] with three levels: (1) damage patterns, (2) damage hypothesis, and (3) parameters inference. This methodology builds on the relative degree of belief of several candidate damage-related model classes that are hierarchically

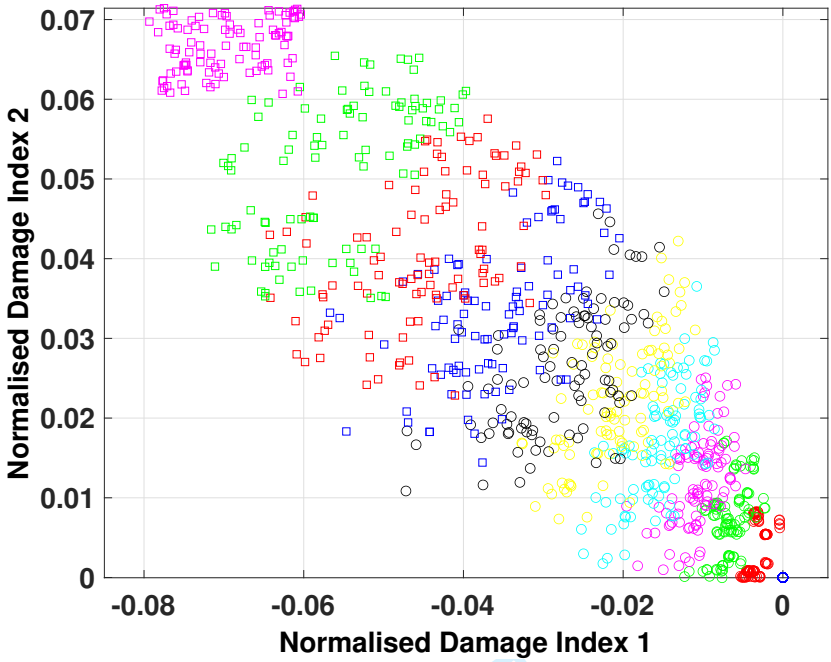

Figure 8. Observation of simulated data based on proposed 'normalised' damage indices (No. of damaged resonators, blue circle: 0; red circle: 1; green circle: 2; magenta circle: 3; cyan circle: 4; yellow circle: 5; black circle: 6; blue square: 7; red square: 8; green square: 9; magenta square: 10)

interdependent. In the context of metamaterials, the global damage is identified as the number of broken resonators, and therefore a damage pattern $\mathbf{M}_j$ (i.e. highest level) can be defined assuming j broken resonators. If the monitored structure has several resonators, a set of damage patterns can be defined as $\mathfrak{M} = \{\mathbf{M}_j\}_{j=1}^{N_p}$ where N_p is the maximum number of broken resonators. In turn, each damage pattern $\mathbf{M}_j$ is described by a set of damage hypotheses $\mathbf{M} = \{\mathcal{M}_i\}_{i=1}^{N_m}$ where N_m is the maximum number of hypotheses. Note that the damage hypothesis $\mathcal{M}_i$ (i.e. middle level) is identified with the location of the i-th missing resonator. Besides, each damage hypothesis or model class is defined by a set of uncertain model parameters $\boldsymbol{\theta}$ along with their prior PDF $p(\boldsymbol{\theta}|\mathcal{M}_i)$. Note also that the evidence (i.e. lowest level) is used in this multilevel approach to rank all the damage hypotheses and patterns [42] as shown below.

Damage patterns: number of broken resonators The ranking of damage patterns, which are related to the number of broken resonators, is obtained by sorting them using their posterior probability given the experimental FRF data $\mathcal{D}$, namely $P(\mathbf{M}_i|\mathcal{D}, \mathfrak{M})$.

This probability is calculated by applying the well-known Bayes' Theorem as follows:

$$P(\mathbf{M}_j|\mathcal{D},\mathfrak{M}) = \frac{p(\mathcal{D}|\mathbf{M}_j)P(\mathbf{M}_j|\mathfrak{M})}{\sum_{k=1}^{N_p} p(\mathcal{D}|\mathbf{M}_k)P(\mathbf{M}_k|\mathfrak{M})} \tag{2}$$

where $P(\mathbf{M}_j|\mathfrak{M})$ is the prior probability of the candidate model class $\mathbf{M}_j$, and $p(\mathcal{D}|\mathbf{M}_j)$ is the evidence of the damage pattern $\mathbf{M}_j$. This evidence can be obtained by applying the Total Probability Theorem as follows:

$$p(\mathcal{D}|\mathbf{M}_j) = \sum_{\ell=1}^{N_p} p(\mathcal{D}|\mathcal{M}_\ell,\mathbf{M}_j)P(\mathcal{M}_\ell|\mathbf{M}_j) \tag{3}$$

Note that Equation (3) defines the evidence of the damage pattern $\mathbf{M}_i$ as a function of the evidences of its damage hypotheses $\mathbf{M} = \{\mathcal{M}_i\}_{i=1}^{N_m}$. Therefore, this creates a bond between the highest and middle levels of this hierarchical Bayesian approach.

Damage hypotheses: Location of a broken resonator Similarly to the damage patterns, the hypotheses can be ranked based on their posterior plausibility conditioned to the same data $\mathcal{D}$ (i.e. $P(\mathcal{M}_j|\mathcal{D},\mathbf{M}_i)$). This probability is defined using the Bayes' Theorem, so that:

$$P(\mathcal{M}_j|\mathcal{D},\mathbf{M}_i) = \frac{p(\mathcal{D}|\mathcal{M}_j,\mathbf{M}_i)P(\mathcal{M}_j|\mathbf{M}_i)}{\sum_{k=1}^{N_p} p(\mathcal{D}|\mathcal{M}_k,\mathbf{M}_i)P(\mathcal{M}_k|\mathbf{M}_i)} \tag{4}$$

where $P(\mathcal{M}_i|\mathbf{M}_j)$ is the prior probability of the i-th damage hypothesis and $p(\mathcal{D}|\mathcal{M}_i,\mathbf{M}_j)$ its evidence, which can be expressed as a function of the model parameters contained in $\mathcal{M}_k$, so $p(\mathcal{D}|\mathcal{M}_i,\mathbf{M}_j) = \int p(\mathcal{D}|\boldsymbol{\theta},\mathcal{M}_i,\mathbf{M}_j)p(\boldsymbol{\theta}|\mathcal{M}_i)d\boldsymbol{\theta}$ where $p(\mathcal{D}|\boldsymbol{\theta},\mathcal{M}_i,\mathbf{M}_j)$ is the likelihood function. This multidimensional integral is usually addressed with Monte Carlo approximation methods given that it typically lacks of analytical solution. However, given that the high probability area of the likelihood and prior PDFs might be unlike, the result of the evidence $p(\mathcal{D}|\mathcal{M}_i,\mathbf{M}_j)$ could be heavily affected by numerical noise [43]. To overcome this limitation, an approach that uses samples from the posterior PDF of the model parameters is adopted in this paper [44, 45].

Parameters inference The lowest level of this Bayesian approach addresses the inference of the uncertain model parameters $\boldsymbol{\theta} \in \boldsymbol{\Theta} \subset \mathbb{R}^{n_\theta}$. To this end, we need the stochastic embedding of the deterministic model that provides predictions about the FRF of a structure $R_{ec}(\boldsymbol{\theta}) \in \mathbb{R}^{n_R}$ (refer to [38]) as a function of $\boldsymbol{\theta}$. The probabilistic description of such a model is achieved by adding a prediction error term $\mathbf{e} \in \mathbb{R}^{n_R}$ that represents the discrepancy between the measured FRF $R_{ec}^{\mathcal{D}}$ and the predicted one:

$$R_{ec}^{\mathcal{D}} = R_{ec}(\boldsymbol{\theta}) + \mathbf{e} \tag{5}$$

The error term is represented here as a zero-mean Gaussian distribution with standard deviation σ_e, given that it provides the largest uncertainty. This is supported by the principle of Maximum Information Entropy [43, 46]. Assuming that the n_R components errors $e_i \in \mathbf{e}$ are independent and identically distributed, the likelihood function is

defined by:

$$p(R_{ec}^{\mathcal{D}}|\boldsymbol{\theta},\mathcal{M}) = \frac{1}{\sqrt{2\pi\sigma_e}^{n_R}} \exp\left(-\frac{1}{2}\sum_{i=1}^{n_R}\left(\frac{R_{ec,i}(\boldsymbol{\theta}) - R_{ec,i}^{\mathcal{D}}}{\sigma_e}\right)^2\right) \tag{6}$$

Then, the posterior information of the model parameters condition to the data $p(\boldsymbol{\theta}|\mathcal{D},\mathcal{M}_j)$ is obtained by updating the prior information using the data $\mathcal{D}$ and the Bayes' Theorem, as follows:

$$p(\boldsymbol{\theta}|\mathcal{D},\mathcal{M}_j) = \frac{p(\mathcal{D}|\boldsymbol{\theta},\mathcal{M}_i)p(\boldsymbol{\theta}|\mathcal{M}_i)}{p(\mathcal{D}|\mathcal{M}_i,\mathbf{M}_j)} \tag{7}$$

where $p(\mathcal{D}|\boldsymbol{\theta},\mathcal{M}_i)$ is the likelihood function previously defined in Equation (6). The set of uncertain model parameters is common for all the damage hypotheses and it is assumed to be defined by $\boldsymbol{\theta} = \{E, \rho, \sigma_e\}$, where E is the Young's modulus and ρ is the density of the printed beams. Note that Equation (7) is addressed using the Metropolis-Hastings (M-H) algorithm [47, 48], which provides samples from the posterior PDF.

Sequential search for damage pattern Identifying the most probable damage pattern leads to a combinatorial problem where the number and location of the broken resonators need to be found. To exhaustively address this optimization problem, the number of candidate damage patterns could be unfeasibly large given the high number of possible combinations of the location of missing resonators. To alleviate this burden, a sequential search strategy based on [49, 50] is adopted to provide an optimal or suboptimal solution for this problem. A pseudo-code of the adopted search approach is shown in Algorithm 1.

Algorithm 1: Bayesian search for the most probable damage pattern

Define $\triangleright\ p(\boldsymbol{\theta}|\mathcal{M})$; // Prior PDF
Define $\triangleright\ N_p,\ N_m$;
Initialize $\triangleright\ \Xi \leftarrow \emptyset$; // Set of damage patterns
for $j = 1$ **to** N_p **do**
  Initialize $\triangleright\ H \leftarrow \emptyset$; // Set of damage hypotheses
  for $i = 1$ **to** N_m **do**
    $H \leftarrow H \cup i$;
    Obtain $p(\boldsymbol{\theta}|\mathcal{D},\mathcal{M}_i)$; // Equation (7)
    Estimate $p(\mathcal{D}|\mathcal{M}_i,\mathbf{M}_j)$;
  end
  Compute $P(\mathcal{M}_i|\mathcal{D},\mathbf{M}_j)$; // Equation (4)
  Find $\mathcal{M}^* = \arg\max_{\mathcal{M}} P(\mathcal{M}_i|\mathcal{D},\mathbf{M}_j)\ \forall i$;
  $\Xi \leftarrow \Xi \cup \mathcal{M}^*$
end
Compute $P(\mathbf{M}_j|\mathcal{D},\mathfrak{M})$; // Equation (2)
Find $\mathbf{M}^* = \arg\max_{\mathcal{M}} P(\mathbf{M}_j|\mathcal{D},\mathfrak{M})\ \forall j$;
Output: $\{\mathbf{M}^*\}$; // Most probable damage pattern

The hierarchical Bayesian approach needs to firstly provide the posterior PDF of the model parameters (Equation (7)) for each of the damage hypotheses (i.e. location of a broken resonator) under the assumption of a damage pattern (i.e. number of broken resonators). Then, all these posterior PDFs are used to compute the posterior probabilities of the damage hypotheses by using Equation (4). The hypothesis with higher probability is chosen as the location of the broken resonator. Finally, when all the damage hypotheses have been explored for all the possible damage patterns, the posterior probabilities of the damage patterns are obtained through Equation (2), and the most probable one is identified.

Data-driven method

In structural health monitoring (SHM), data-driven approaches (i.e., machine learning [36]) are often used to detect and classify structural damage. In general, this requires clustering the data into groups corresponding to different health states of the investigated structure. In literature, various methods haven been employed, including support vector machines [51] and artificial neural networks [52]. Considering the damage characteristics of metamaterial beams discussed in the last section, inferring the damage level through a probabilistic manner instead of finding hard boundaries for different clusters is preferred. Since the training data are labelled, a simple fully-supervised data-driven model is applied in this work. Specifically, assuming that each cluster of data are Gaussian distributed. The mean and covariance of each class can be determined based on the sample mean and covariance of training data. The number of damaged resonators for a test data D then can be inferred based on the posterior PDFs of the test data belonging to each damage class, providing a probabilistic estimation of the damage level. That is:

$$\begin{aligned} p\left(C_i \,|D\right) &= \mathcal{N}\left(D\,|\mu_i,\, \mathbf{\Sigma}_i\right) \\ &= \det\left(2\pi\Sigma_i\right)^{-1/2} \exp\left(-\frac{1}{2}(D-\mu_i)^{\mathrm{T}}\Sigma_i^{-1}\left(D-\mu_i\right)\right) \end{aligned} \tag{8}$$

where C_i $(i = 1..M)$ denotes the damage class; μ_i and $\mathbf{\Sigma}_i$ denote the estimated mean and covariance of this damage class.

A straightforward classification method is employed in this work. This is due to the fact that the main aim here is not to infer complex functional descriptions on the clustering boundaries, but to properly account for the uncertainties among different test samples.

Results and Discussion

Both numerical and experimental data examples are presented in this section to assess the damage identification and quantification quality based on the methods mentioned in the last section.

Numerical results based on the Bayesian inverse method

The proposed methodology is numerically assessed considering a beam with ten unit cells and one pair of resonators per unit cell. Two numerical case studies are designed by assuming that the experimental data $\mathcal{D}$ is numerically obtained from the response of the beam with damage in: (1) the 6-th unit cell, and (2) the 4-th and 6-th unit cells. Note that these case studies are for illustration purposes of the Bayesian methodology, and only two examples with one and two missing resonators are shown.

For the multilevel Bayesian damage identification approach, the prior distributions of each of the uncertain parameters $p(\boldsymbol{\theta}|\mathcal{M})$ have been chosen to be as follows (based on 17) : Young's modulus normally distributed as $E \sim \mathcal{N}(1621.7, 49.90^2)$ in MPa, density normally distributed as $\rho \sim \mathcal{N}(948.96, 7.39^2)$ in kg/m^3, and standard deviation of the prediction error uniformly distributed as $\sigma_e \sim \mathcal{U}(0.01, 10)$. These prior PDFs are defined according to the measured distribution of the values of E and ρ in real experiments. Note that these prior distributions are used for both numerical case studies.

One broken resonator The accuracy of Bayesian approach is firstly evaluated using the data $\mathcal{D}$ stemming from ten unit cell beam with a broken resonator in the 6-th unit cell. Therefore, the number of possible damage patterns and damage hypotheses per pattern are defined to be $N_p = N_m = 10$. The M-H algorithm is run using $20,000$ samples and a Gaussian proposal distribution. The standard deviation of the proposal distribution is appropriately selected so that the acceptance rate is within the interval $[0.2, 0.4]$ [53, 45].

Figure 9 depicts the results obtained from the multilevel Bayesian inverse problem. Figure 9b shows that the most probable damage pattern is the one that assumes one broken resonator with a posterior probability of $P(\mathbf{M}_1|\mathcal{D}, \mathfrak{M}) = 32.32\%$. The corresponding most plausible damage location (or damage hypothesis) is obtained at the 6-th unit cell with a probability $P(\mathcal{M}_6|\mathcal{D}, \mathbf{M}_1) = 20.35\%$, as shown in Figures 9a and 9c. Therefore, the identified damage pattern matches with the modelled one. However, it is worth mentioning that probability mass distribution of the damage hypothesis is almost symmetric with respect to the geometrical center of the beam. This could lead to misidentification if the posterior probabilities of the hypotheses, hence their evidences, are not properly calculated.

Two broken resonators This case study considers two broken resonators in the 4-th and 6-th unit cells of the beam, and therefore the data $\mathcal{D}$ is numerically obtained in this scenario. Note that the damage patterns, hypotheses, and the M-H algorithm are equally configured as the first case study. The most probable damage pattern results to be $\mathbf{M}_2$ with a posterior probability of $P(\mathbf{M}_2|\mathcal{D}, \mathfrak{M}) = 30.15\%$ as can be observed in Figure 10b. For illustration purposes, the results obtained for the first damage pattern $\mathbf{M}_1$ are shown in Figure 10. Figures 10a and 10c represent the probability mass distribution considering one broken resonator, i.e. $P(\mathcal{M}_i|\mathcal{D}, \mathbf{M}_1)$.The most probable damaged location results to be the 6-th unit cell with a posterior probability of $P(\mathcal{M}_6|\mathcal{D}, \mathbf{M}_1) = 24.10\%$, which partially matches with the original damage.

The results obtained for the second and most probable damage pattern $\mathbf{M}_2$ are shown in Figure 11. This damage pattern is built by the union of the previously selected damage

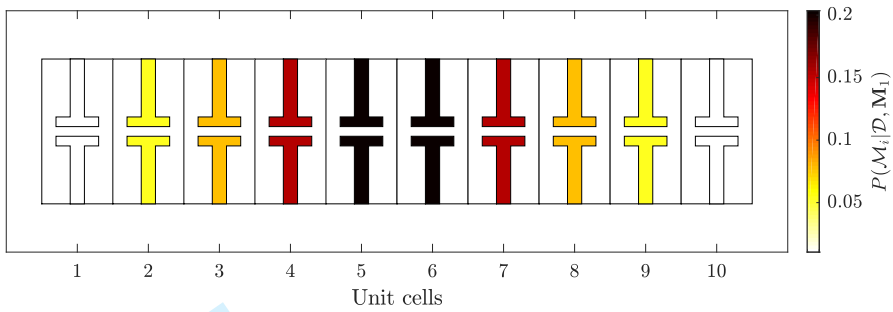

(a) Graphical representation of the damage hypotheses for the first pattern, $P(\mathcal{M}_i|\mathcal{D},\mathbf{M}_1)$.

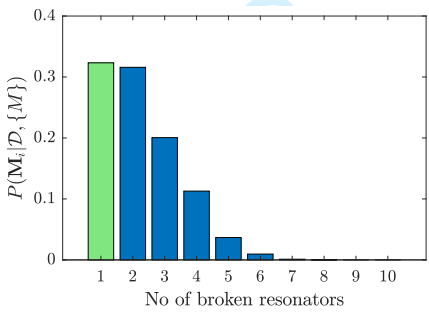

(b) $P(\mathbf{M}_i|\mathcal{D},\mathfrak{M})$

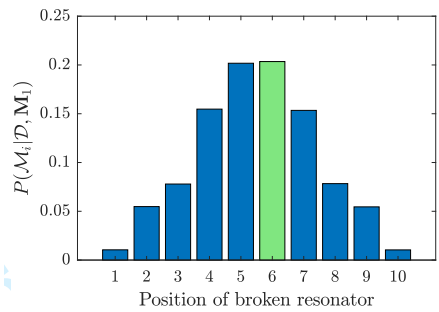

(c) $P(\mathcal{M}_i|\mathcal{D},\mathbf{M}_1)$

Figure 9. Damage identification results from the first numerical case study considering one broken resonator and the multilevel Bayesian approach. Panel (a) and (c): spatial representation and bar graph of the posterior probability of damage hypotheses in $\mathbf{M}_1$. Panel (b): posterior probabilities of the candidate damage patterns in $\mathfrak{M}$.

hypothesis $\mathcal{M}_6$ and a new candidate. Note that the 6-th unit cell is represented in gray in Figure 11a to show that is fixed in this second stage of the sequential search algorithm. The probability mass function of the damage hypotheses $P(\mathcal{M}_i|\mathcal{D},\mathbf{M}_2)$ is depicted in Figures 11a and 11c. Note also that the most probable damaged resonator would lie in the 4-th unit cell (i.e. $P(\mathcal{M}_4|\mathcal{D},\mathbf{M}_2) = 19.10\%$), although a symmetry effect is again identified between the 4-th and 7-th unit cells.

The identification of the number of broken resonators in the beam has been accurately obtained with both numerical cases studies. Additionally, the localization of damage has been properly obtained. However, it shows a less identifiable scenario as observed from the probability mass distributions of the damage hypotheses in Figures 9c, 10c, and 11c. The similar mechanical behavior of the beam when removing resonators at symmetric locations make the response to be alike and the damage hypothesis less identifiable. In fact, for real experiments, this limitation could be further strengthen given that further uncertainties and noise in the data will be present. To address this challenging scenario, one desirable extension of the multilevel Bayesian framework would be to introduce

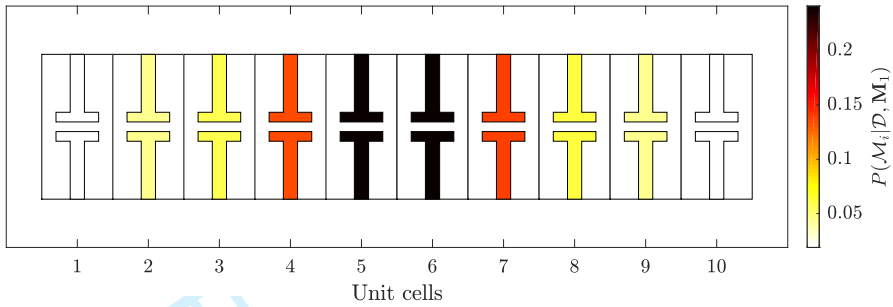

(a) Graphical representation of the first most probable broken resonator $P(\mathcal{M}_i|\mathcal{D},\mathbf{M}_1)$.

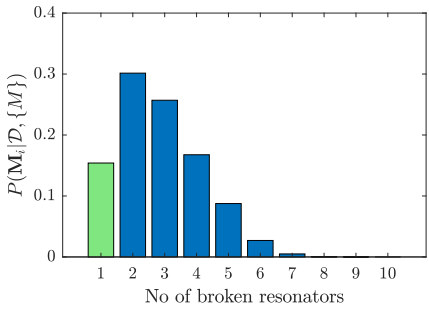

(b) $P(\mathbf{M}_i|\mathcal{D},\mathfrak{M})$

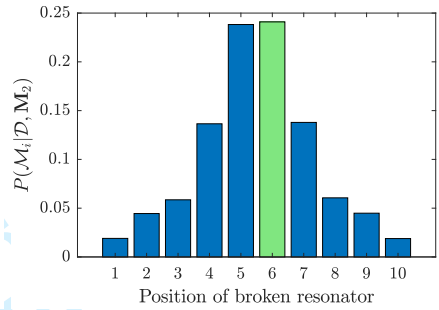

(c) $P(\mathcal{M}_i|\mathcal{D},\mathbf{M}_1)$

Figure 10. Results from the second numerical case study considering two broken resonators. Panel (a) and (c): spatial representation and bar graph of the posterior probability of damage hypotheses in $\mathbf{M}_1$. Panel (b): posterior probabilities of the candidate damage patterns in $\mathfrak{M}$.

further uncertain physical parameters in $\boldsymbol{\theta}$ from the FRF model, such as the attenuation or the thickness of the printed walls. This could provide further sensitivity for specific unit cells and make the damage hypotheses more easily identifiable.

Numerical results based on data driven method

Based on the proposed damage indices, the quality of damage quantification using the exhibited data-driven method is numerically assessed in this section. One hundred metamaterial beams have been generated as training data. (Although details are omitted here, investigation on the effect of sampling number has been conducted and it is shown that one hundred samples are sufficient for analysis balancing accuracy and efficiency.) The Young's modulus and density of each sample are randomly generated based on the distribution of $E \sim \mathcal{N}(1621.7, 49.90^2)$ in MPa and $\rho \sim \mathcal{N}(948.96, 7.39^2)$ in kg/m^3. The damage conditions are then simulated by removing one to ten resonators with randomly picked locations, leading to one thousand data points in total. An independent

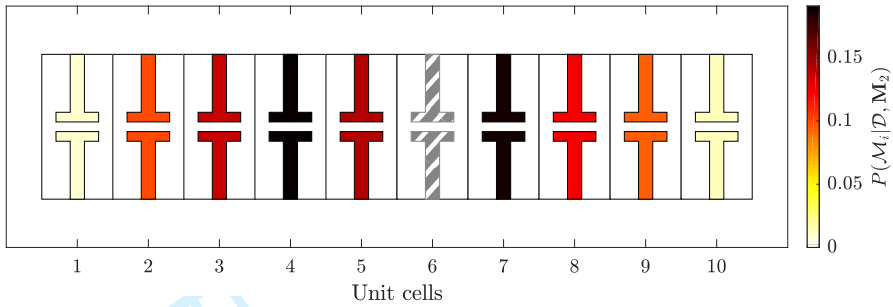

(a) Graphical representation of the second most probable broken resonator $P(\mathcal{M}_i|\mathcal{D},\mathbf{M}_2)$.

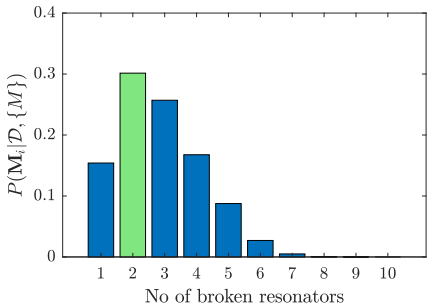

(b) $P(\mathbf{M}_i|\mathcal{D},\mathfrak{M})$

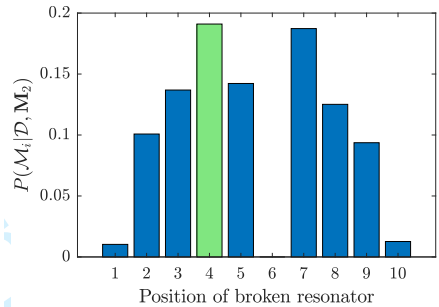

(c) $P(\mathcal{M}_i|\mathcal{D},\mathbf{M}_2)$

Figure 11. Results from the second numerical case study considering two broken resonators. Panel (a) and (c): spatial representation and bar graph of the posterior probability of damage hypotheses in $\mathbf{M}_2$. In this damage pattern, the 6-th is initially considered as broken, as extracted from Figure 10. Panel (b): posterior probabilities of the candidate damage patterns in $\mathfrak{M}$.

experimental dataset has also been generated through the same procedure with 10 sample beams (i.e., 100 data points in total) as described above.

Figure 12 shows the clusters based on the training data. The overall accuracy based on the test dataset is about 67%, which is not acceptable from first glance. Since a soft clustering method is applied in this example, posterior PDFs of a tested case for all damage classes are available. Detailed investigation of these posterior PDFs shows that the damaged samples are mainly misclassified to the neighbouring damage numbers. Figure 13 shows the confusion matrix (i.e., posterior PDFs of all damaged classes) of a test beam as a typical case. It can be seen that the highest posterior pdfs are distributed around ± 1 of the true number of damaged resonators. This is reasonable since the neighbouring damaged cases are quite overlaid. Changing the damage quantification criteria to ± 1 of damaged resonators, the overall accuracy can be increased to 100%.

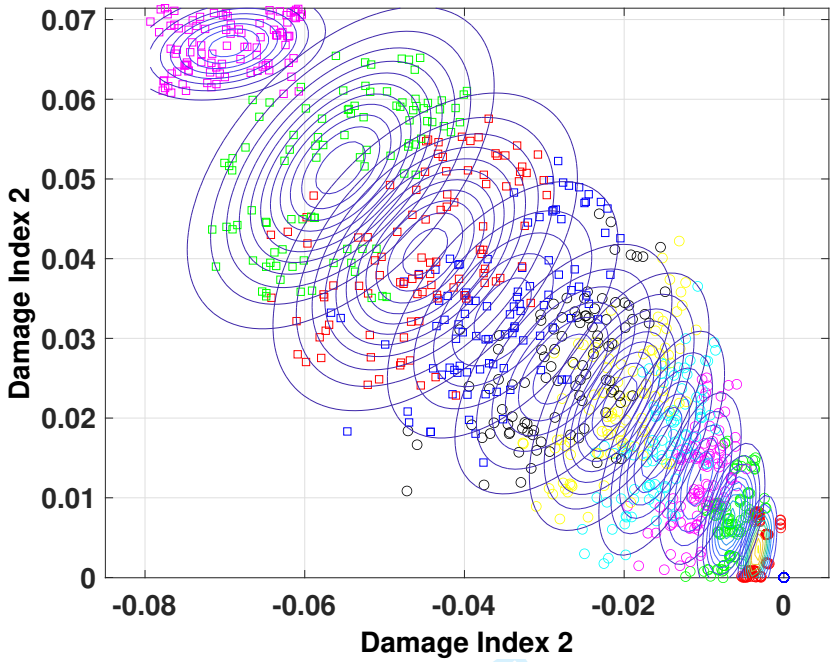

Figure 12. Observation of simulated data based on proposed 'normalised' damage indices with clusters (No. of damaged resonators, blue circle: 0; red circle: 1; green circle: 2; magenta circle: 3; cyan circle: 4; yellow circle: 5; black circle: 6; blue square: 7; red square: 8; green square: 9; magenta square: 10. Corresponding clusters are overlaid on the top of each damage class)

Other advanced data driven classification methods have also been applied for comparison, including support vector machine (SVM) [54], k-nearest neighbors (KNN) [55], linear discriminant analysis (LDA) [56] and complex tree [57]. MATLAB classification learner has been used to deploy these methods with default settings. (Specifically, quadratic SVM, fine KNN with the number of neighbors set to be 1 and find tree with maximum number of splits set to be 100 are used.) Details are omitted while the quantification results are shown in Table 2. It can be seen that applying advanced methods does not provide much improvements in performance. This is reasonable due to the nature of the investigated resonant metamaterials. The geometrical and material uncertainties among samples are significant and the samples with different damage conditions are quite overlaid. The major difficulty here is to properly account for such uncertainties instead of finding complex clustering boundaries. The performance will become even worse when applying to experimental data with limited training data and measurement noise. Through balanced accuracy and efficiency, the simple damage quantification method used in this work is sufficient for damage quantification purposes.

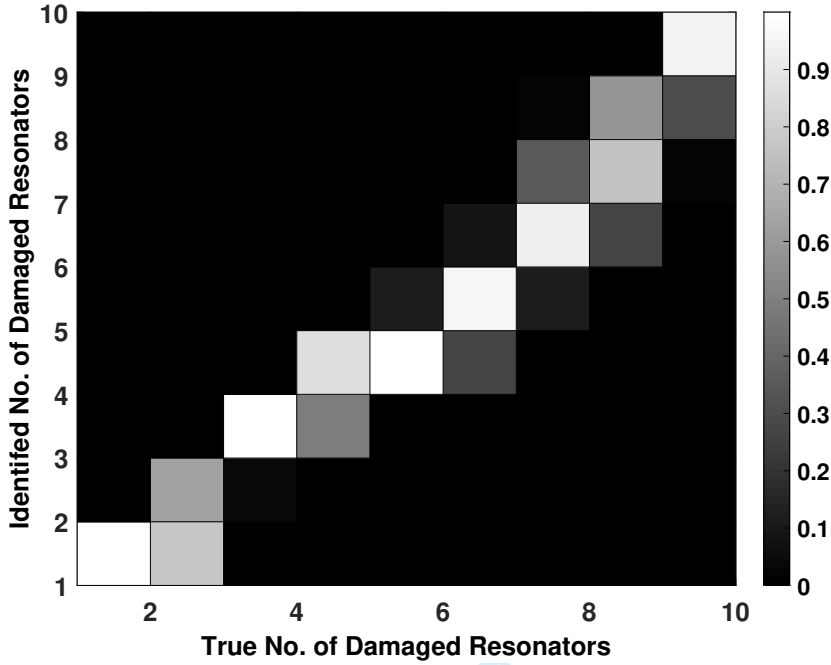

Figure 13. Confusion matrix of a test sample beam, numerical example

Table 2. Accuracy of other classification methods

Methods	SVM	KNN	LDA	Complex Tree
Accuracy (%)	79.1	69.1	70.9	72.7

Experimental Results

The proposed damage indices and soft clustering method are applied to experimental data, hereby presented in this section. Figure 14 shows the realisation of the experimental samples based on the proposed damage indices. It can be seen that the data are more divergent compared to the numerical dataset. This is reasonable due to the uncertainty involved during manufacturing as well as induced by measurement noise. Furthermore, the number of experimental samples are also limited, which is ten in this work. It is much more difficult to get a properly trained data-driven model in this case. In view of this, the overall quality of the damage quantification method is assessed by randomly picking one sample beam as test beam and using the data from remaining beams for training, leading to 10 different cases in total (each corresponding to a different number of broken resonators). The overall damage quantification accuracy of the proposed data-driven method ranges from 40% to 90% with an averaged value of 61%.

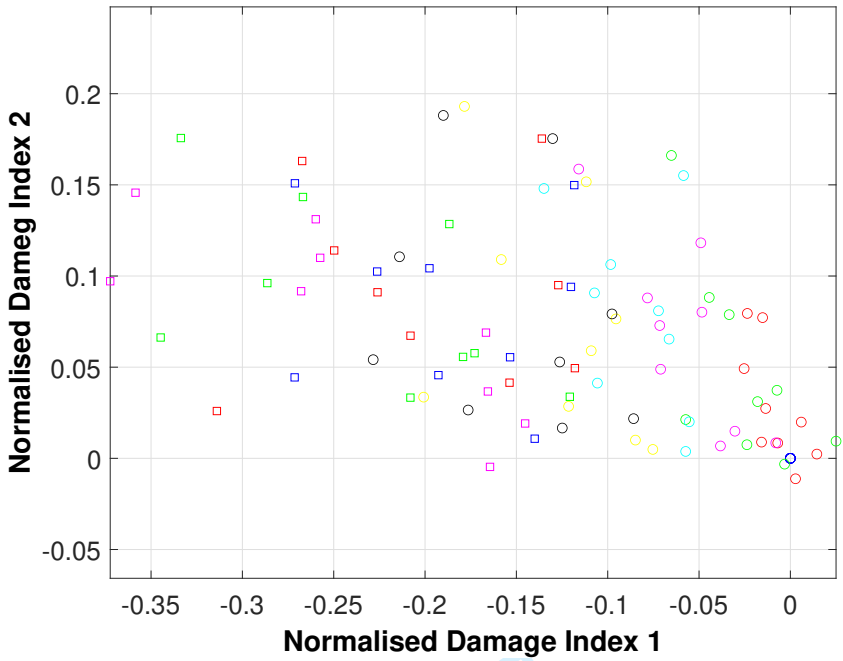

Figure 14. Observation of experimental data based on proposed 'normalised' damage indices (No. of damaged resonators, blue circle: 0; red circle: 1; green circle: 2; magenta circle: 3; cyan circle: 4; yellow circle: 5; black circle: 6; blue square: 7; red square: 8; green square: 9; magenta square: 10)

Figure 15 shows the confusion matrix of a test beam as a typical case. Similar to the numerical example, high posterior PDFs are mainly distributed around the neighbouring classes. However, the misclassification range for experimental data is wider than numerical data (which are mainly misclassified within ± 1 resonator). This is reasonable since the number of training data is extremely limited and more manufacture and measurement uncertainties are involved.

Remarks on presented results

As exhibited in the case studies above, the proposed damage indices are capable of reducing the effect of variation between test samples due to uncertainty. Compared to outputs for the numerical dataset, quantifying the damaged resonators in experimental samples based purely on the data-driven method can still be challenging due to the limited number of training data and more uncertainty involved which cannot be controlled. Recently, the idea of transfer learning has been applied to structural health monitoring in order to deal with the situation when training and testing datasets are obtained from

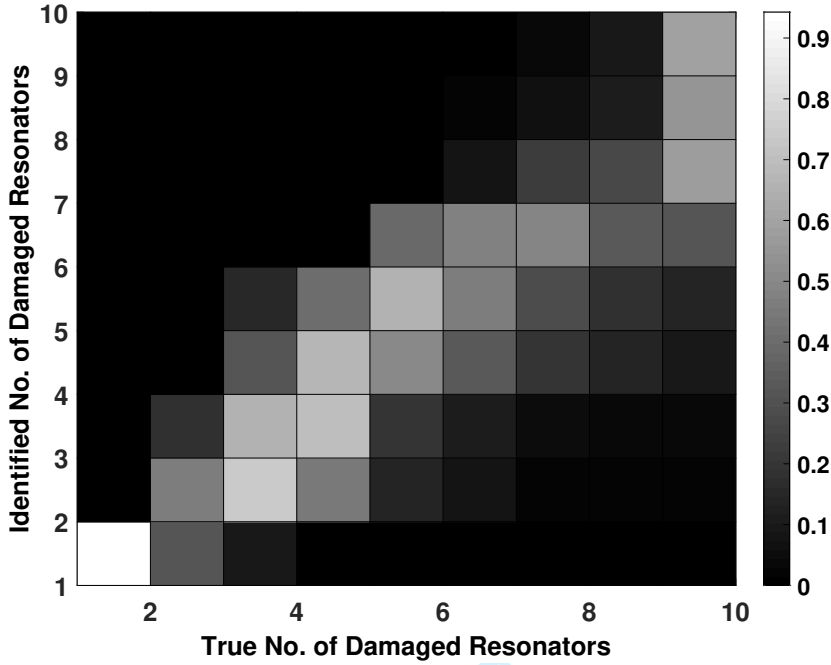

Figure 15. Confusion matrix of a test sample beam, experimental example

two different systems [58]. By projecting these two datasets to the same domain where they are overlaid, one clustering strategy can be applied. This opens the possibility of fusing numerical and experimental datasets for damage identification. Having said that, this is still an open fundamental problem which needs to be tackled in the decades to come. Instead of quantifying the exact number of damaged resonators, the data driven method based on the proposed damage indices in this work provides a good estimation on a possible range of damaged resonators for both numerical and experimental data. It is expected that having a larger training dataset could improve the quantification results.

Compared to the data-driven method, the multi-level probabilistic Bayesian approach provides a rigorous way of not only quantifying but also localising the damaged resonators with quantified uncertainty. However, one main issue of this method is that it requires a well calibrated model (i.e., the system parameters should be accurately identified during the process) in order to provide reasonable inference on damage patterns and hypotheses, which is not needed for data driven methods. When the involved uncertainties (e.g., geometrical and material uncertainties of the experimental samples) are significant, identifiability problems can be encountered, leading the calibration issues of the system model that cannot be overcome.

As the uncertainty of the experimental resonant metamaterials is rather high, a relatively large discrepancy between experimental FRF data and model predictions has been obtained. This has caused insurmountable issues regarding the model calibration in undamaged conditions, which has ultimately leaded to the inability to use the multi-level Bayesian approach along with the experimental data. To further investigate the reasons of this apparent limitation, a global sensitivity analysis (GSA) [59] of the FRF model has been performed. Thus, the total effect index T_i of the i-th model parameter, which gives the relative importance of the i-th parameter in the model output, can be obtained as follows [60]:

$$T_i = \frac{E(V(Y|\mathbf{X}_{-i}))}{V_Y} \tag{9}$$

where $E(V(Y|\mathbf{X}_{-i}))$ is the remaining variance of Y (i.e. the model output) in case the value of the $\mathbf{X}_{-i}$ (i.e. all the parameters except X_i) are known; and V_Y denotes the total unconditional variance of the model. The calculation of these indices is computationally challenging, but approximate methods have been adopted to reduce the computational burden [61].

In this case, a set of 5 potential model parameters are investigated, namely $\mathbf{X} = \{E, \rho, \eta, w_d, H_d\}$. The parameters are assumed to be normally distributed as follows: E and ρ have the experimental distribution described in 17, while η, w_d, and H_d are centered in their nominal value given in the second section with a standard deviation of a 10% of the mean value. The model output is evaluated within the frequency range of $[200, 600]$ Hz, and 1e+6 samples are used to estimate the total effect indices, while checking its convergence. The resulting indices are shown in Figure 16, where both the Young's modulus E and the beam height H_d are found to be the most sensitive parameters

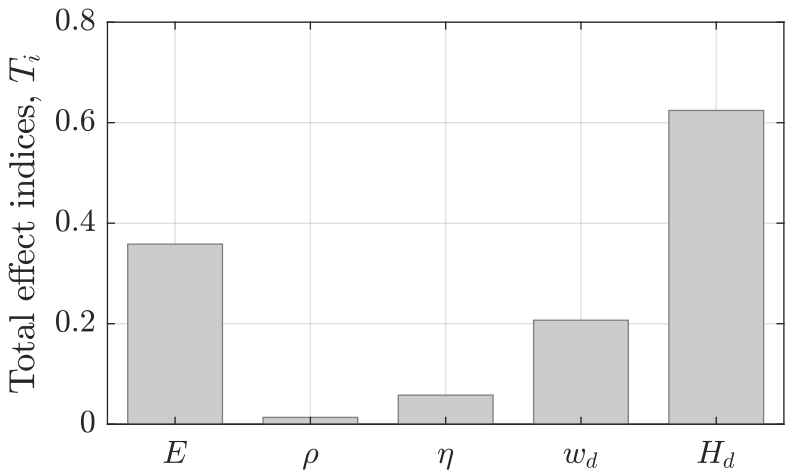

Figure 16. Total effect indices for the set of 5 model parameters $\mathbf{X} = \{E, \rho, \eta, w_d, H_d\}$.

From this standpoint, and to provide further insight into the Bayesian approach limitation when using the experimental data, the overall variance V_Y of the model is compared against the one extracted from the experimental data of the 12 metamaterial beams in undamaged state. Thus, the model variance is $V_Y = 1.10\text{e+}4$, while the experimental variance is $1.21\text{e+}4$. This shows that the variance of the experimental data is higher than the model variance, which makes it difficult to have a well calibrated model in the first place to address the identification. This is the main reason why the Bayesian approach has not been able to deal with the available experimental data. To overcome this issue, a larger dataset would indeed be needed to obtain a calibrated model that could in turn provide more information about damage patterns and hypotheses in metamaterial beams.

Conclusions

This work investigated the plausibility of damage identification and quantification in resonant metamaterials based on their FRF data. The properties of FRFs with broken resonators have been investigated and the challenges in damage identification and quantification due to material and geometrical uncertainties were discussed. Damage indices have been proposed in this work to suppress the effect due to such uncertainties. Based on the proposed damage indices, a data-driven method has been implied to infer the number of damaged resonators. At the same time, a physics-based Bayesian inverse methodology was developed and applied to explore the feasibility of localising the damaged resonators. Both methods were validated using numerical simulations. The feasibility of applying the methods to experimental data has also been investigated. It is possible to provide reasonable estimation on the damage states of the experimental resonant metamaterials but more challenging compared to numerical data. It was shown that the quality of the data-driven method highly depends on the training data set, which is rather limited for experimental samples. On the other hand, the Bayesian inverse method is capable of inferring the location of damaged resonators without the need of large training datasets. However, to enhance accuracy of estimations, the properties of the tested samples should be well-known, which cannot be guaranteed for resonant metastructures manufactured through 3D printed processes.

This work also leads to several research topics that are worth investigating in future. First, this paper focuses on situations where the damaged resonators are located in the middle of the beam due to the fact that these resonators are more likely to encounter damage in industrial applications. However, the proposed methods in this work are generally applicable to all resonators. Additional experiments for damaged resonators located at two ends can be conducted to further validate the efficiency of the methods.Second, it is currently challenging to distinguish the situations when the damaged resonators are symmetric. Additional uncertainty parameters such as attenuation or thickness of the printed walls should be introduced to provide sensitivity for specific resonators, which requires further research.

Acknowledgements

This paper is part of the SAFE-FLY project that has received funding from the European Union's Horizon 2020 research and innovation programme under the Marie Skłodowska-Curie grant agreement No.721455. The authors would also like to acknowledge the support acquired by Natural Science Foundation of Jiangsu Province (Project No.BK20220853), High Level Personnel Project of Jiangsu Province (Project No. JSSCBS20210154), the H2020 DiaMoND project under the Marie Skłodowska-Curie grant agreement No.785859 and the Science and Technology Development Fund, Macau SAR (File no. SKL-IOTSC(UM)-2021-2023, 0101/2021/A2, 0010/2021/AGJ).

Appendix

Experimental uncertainty quantification of the 3D printed material properties

In order to measure the density and flexural modulus variability 15 beams with dimensions of 10mm×4mm×80mm were manufactured by the Selective Laser Sintering method and experimentally manipulated. The densities of the beams were calculated with their masses and volumes, which were measured by a precision scale and a caliper. The flexural modulus was measured by the Instron universal testing machine 6800 SERIES with the employment of the 3-point testing method following the standard ASTM D790-17 as shown in Figure A.1.
The flexural modulus can be obtained by

$$E = \frac{D_s^3 m_x}{4 b_x h_x^3} \tag{10}$$

where D_s is the distance between two supports, b_x and h_x are the widths and heights of the tested beams and m_x is slope at the initial straight-line portion of the load-deflection curve.

Figure A.2 shows the measured densities and flexural moduli, while their mean values and standard deviations are given in Table A.1.

Table A.1. Mean values and standard deviations of the density and flexural modulus of the tested beams

	Density (kg/m^3)	Elastic modulus (MPa)
Mean values	948.9	1621.7
Standard deviations	7.4	49.9

Uniform design of the experiment

In real applications, the efficiency and accuracy of damage assessment methods depends critically on the design of the experiment, whose objective is to establish an unknown

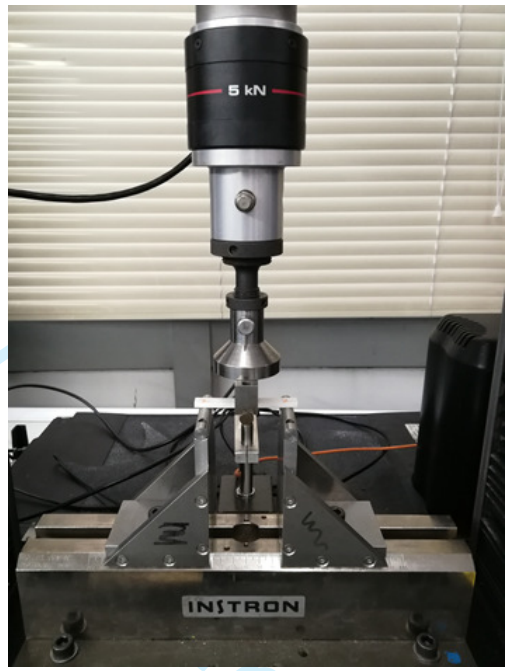

Figure A.1. Universal test machine with the tested beam sample for flexural modulus testing.

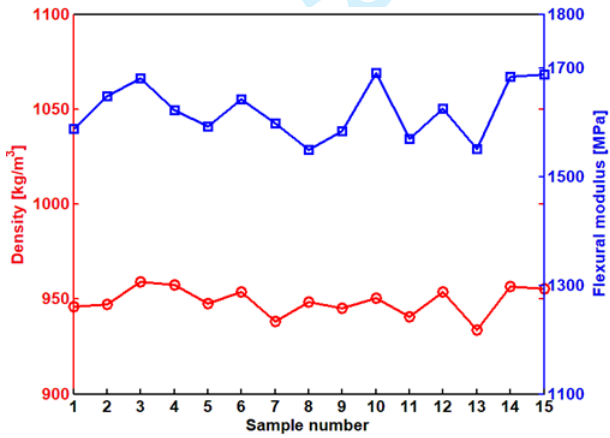

Figure A.2. Measured densities and flexural moduli of the 3D printed beams.

relationship between the response (output) and factors (input) with a realistic number of experiments. Unfortunately, with an increasing number of factors, the required number

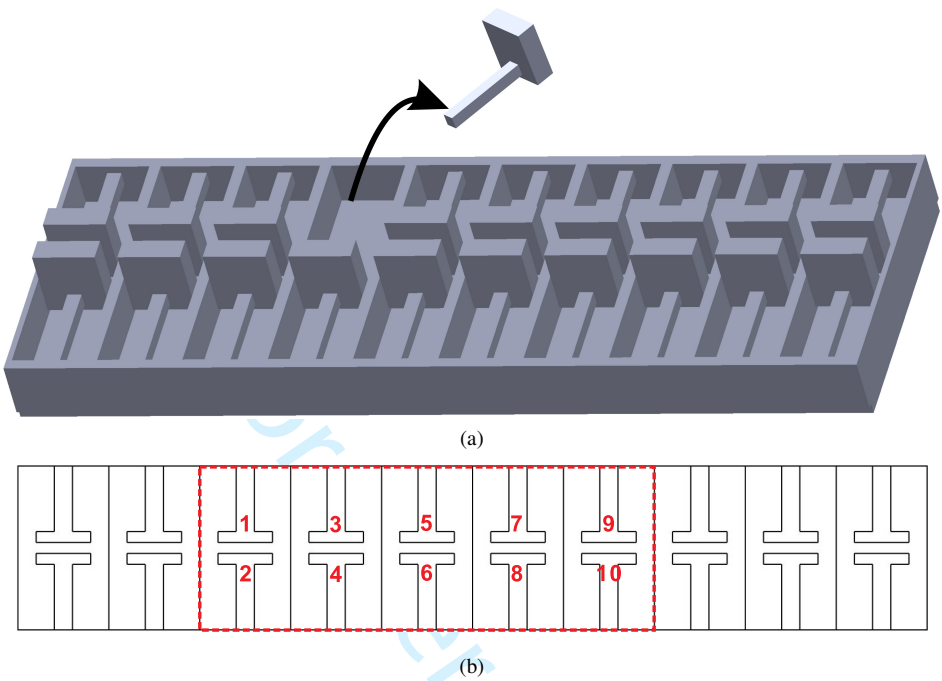

Figure A.3. (a) Schematic of resonator removal from the beam, (b) locations of the removed resonators in the experimental tests

of experiments increase exponentially in classical experimental designs. Therefore, one should resort to modern experimental designs by using a small number of experiments to explore relationships between the response and the factors. The uniform design proposed by Fang et al. [62] is an efficient fractional factorial design scheme. Uniform design has often been adopted to seek a reasonable number of design points that are uniformly scattered in the domain in order to achieve the necessary accuracy. In this work, 10 resonant metamaterial samples are tested to investigate the effect of damaged resonators on the FRFs. For each sample, 10 resonators were removed one-by-one from the beam as shown schematically in Figure A.3(a). Uniform design has been applied in this work to determine the sequence of the removed resonators for each sample when conducting the experiment tests, which is shown in Table A.2. The corresponding locations of these removed resonators are shown in Figure A.3(b). Experimental tests focus on the situations where damaged resonators are located at the middle of the test samples. This is because resonators at the middle are more likely to encounter damage than those at two edges in industrial applications.

Table A.2. Sequence of the removed resonators for the experimental tests based on the uniform design

Run	Damaged resonator No.									
1	7	8	4	5	3	3	10	4	7	8
2	9	2	5	7	2	9	3	6	10	3
3	2	5	6	1	10	6	4	5	9	6
4	1	7	7	10	1	7	8	9	6	2
5	3	6	1	8	6	8	5	3	8	10
6	4	10	10	2	9	10	6	2	2	7
7	10	4	2	3	5	1	7	10	4	4
8	5	3	9	9	8	4	1	8	5	1
9	8	9	3	4	4	2	2	7	3	5
10	6	1	8	6	7	5	9	1	1	9

References

[1] Cai W, Chettiar UK, Kildishev AV et al. Optical cloaking with metamaterials. *Nature photonics* 2007; 1(4): 224–227.

[2] Alkurt FO, Altintas O, Ozakturk M et al. Enhancement of image quality by using metamaterial inspired energy harvester. *Physics Letters A* 2020; 384(1): 126041.

[3] Cummer SA, Christensen J and Alù A. Controlling sound with acoustic metamaterials. *Nature Reviews Materials* 2016; 1(3): 1–13.

[4] Wang S, Feresidis AP, Goussetis G et al. High-gain subwavelength resonant cavity antennas based on metamaterial ground planes. *IEE Proceedings-Microwaves, Antennas and Propagation* 2006; 153(1): 1–6.

[5] Ungureanu B, Achaoui Y, Enoch S et al. Auxetic-like metamaterials as novel earthquake protections. *arXiv preprint arXiv:151008785* 2015; .

[6] Craster RV and Guenneau S. *Acoustic metamaterials: Negative refraction, imaging, lensing and cloaking*, volume 166. Springer Science & Business Media, 2012.

[7] Yan Y, Cheng L, Wu Z et al. Development in vibration-based structural damage detection technique. *Mechanical systems and signal processing* 2007; 21(5): 2198–2211.

[8] An YK and Sohn H. Integrated impedance and guided wave based damage detection. *Mechanical Systems and signal processing* 2012; 28: 50–62.

[9] Su Z, Ye L and Lu Y. Guided lamb waves for identification of damage in composite structures: A review. *Journal of sound and vibration* 2006; 295(3-5): 753–780.

[10] Yan WJ, Chronopoulos D, Papadimitriou C et al. Bayesian inference for damage identification based on analytical probabilistic model of scattering coefficient

estimators and ultrafast wave scattering simulation scheme. *Journal of Sound and Vibration* 2020; 468: 115083.

[11] Yan WJ, Chronopoulos D, Cantero-Chinchilla S et al. A fast bayesian inference scheme for identification of local structural properties of layered composites based on wave and finite element-assisted metamodeling strategy and ultrasound measurements. *Mechanical Systems and Signal Processing* 2020; 143: 106802.

[12] Farrar CR, Doebling SW and Nix DA. Vibration–based structural damage identification. *Philosophical Transactions of the Royal Society of London Series A: Mathematical, Physical and Engineering Sciences* 2001; 359(1778): 131–149.

[13] Xia Y, Hao H, Zanardo G et al. Long term vibration monitoring of an rc slab: temperature and humidity effect. *Engineering structures* 2006; 28(3): 441–452.

[14] Salawu O. Detection of structural damage through changes in frequency: a review. *Engineering structures* 1997; 19(9): 718–723.

[15] Maia N, Silva J, Almas E et al. Damage detection in structures: from mode shape to frequency response function methods. *Mechanical systems and signal processing* 2003; 17(3): 489–498.

[16] Yan WJ, Ren WX and Huang TL. Statistic structural damage detection based on the closed-form of element modal strain energy sensitivity. *Mechanical Systems and Signal Processing* 2012; 28: 183–194.

[17] Ni Y, Zhou H, Chan K et al. Modal flexibility analysis of cable-stayed ting kau bridge for damage identification. *Computer-Aided Civil and Infrastructure Engineering* 2008; 23(3): 223–236.

[18] Sampaio R, Maia N and Silva J. Damage detection using the frequency-response-function curvature method. *Journal of sound and vibration* 1999; 226(5): 1029–1042.

[19] Yan WJ, Zhao MY, Sun Q et al. Transmissibility-based system identification for structural health monitoring: fundamentals, approaches, and applications. *Mechanical Systems and Signal Processing* 2019; 117: 453–482.

[20] Sampaio R and Maia N. Strategies for an efficient indicator of structural damage. *Mechanical Systems and Signal Processing* 2009; 23(6): 1855–1869.

[21] Esfandiari A. Structural parameter estimation and damage detection using experimental transfer function data. *Inverse Problems in Science and Engineering* 2020; 28(1): 2–20.

[22] Esfandiari A, Rahai A, Sanayei M et al. Model updating of a concrete beam with extensive distributed damage using experimental frequency response function. *Journal of Bridge Engineering* 2016; 21(4): 04015081.

[23] Esfandiari A, Bakhtiari-Nejad F, Rahai A et al. Structural model updating using frequency response function and quasi-linear sensitivity equation. *Journal of sound and vibration* 2009; 326(3-5): 557–573.

[24] Vahedi M, Khoshnoudian F, Hsu TY et al. Transfer function-based bayesian damage detection under seismic excitation. *The Structural Design of Tall and Special Buildings* 2019; 28(12): e1619.

[25] Worden K, Cross EJ, Dervilis N et al. Structural health monitoring: from structures to systems-of-systems. *IFAC-papersonline* 2015; 48(21): 1–17.

[26] Friswell MI. Damage identification using inverse methods. *Philosophical Transactions of the Royal Society A: Mathematical, Physical and Engineering Sciences* 2007; 365(1851): 393–410.

[27] Farrar CR and Worden K. *Structural health monitoring: a machine learning perspective*. John Wiley & Sons, 2012.

[28] Law S, Li X, Zhu X et al. Structural damage detection from wavelet packet sensitivity. *Engineering structures* 2005; 27(9): 1339–1348.

[29] Fan X, Li J, Hao H et al. Identification of minor structural damage based on electromechanical impedance sensitivity and sparse regularization. *Journal of Aerospace Engineering* 2018; 31(5): 04018061.

[30] Hou R, Xia Y and Zhou X. Structural damage detection based on l1 regularization using natural frequencies and mode shapes. *Structural Control and Health Monitoring* 2018; 25(3): e2107.

[31] Beck JL and Katafygiotis LS. Updating models and their uncertainties. i: Bayesian statistical framework. *Journal of Engineering Mechanics* 1998; 124(4): 455–461.

[32] Yuen KV. *Bayesian methods for structural dynamics and civil engineering*. John Wiley & Sons, 2010.

[33] Yan WJ and Katafygiotis LS. A novel bayesian approach for structural model updating utilizing statistical modal information from multiple setups. *Structural Safety* 2015; 52: 260–271.

[34] Yan WJ and Katafygiotis LS. Application of transmissibility matrix and random matrix to bayesian system identification with response measurements only. *Smart Materials and Structures* 2016; 25(10): 105017.

[35] Figueiredo E, Park G, Farrar CR et al. Machine learning algorithms for damage detection under operational and environmental variability. *Structural Health Monitoring* 2011; 10(6): 559–572.

[36] Worden K and Manson G. The application of machine learning to structural health monitoring. *Philosophical Transactions of the Royal Society A: Mathematical, Physical and Engineering Sciences* 2007; 365(1851): 515–537.

[37] Cross E, Manson G, Worden K et al. Features for damage detection with insensitivity to environmental and operational variations. *Proceedings of the Royal Society A: Mathematical, Physical and Engineering Sciences* 2012; 468(2148): 4098–4122.

[38] Meng H, Chronopoulos D, Fabro A et al. Rainbow metamaterials for broadband multi-frequency vibration attenuation: Numerical analysis and experimental validation. *Journal of Sound and Vibration* 2020; 465: 115005.

[39] Meng H, Chronopoulos D, Fabro AT et al. Optimal design of rainbow elastic metamaterials. *International Journal of Mechanical Sciences* 2020; 165: 105185.

[40] Fabro AT, Meng H and Chronopoulos D. Uncertainties in the attenuation performance of a multi-frequency metastructure from additive manufacturing. *Mechanical Systems and Signal Processing* 2020; 138: 106557.

[41] Wold S, Esbensen K and Geladi P. Principal component analysis. *Chemometrics and intelligent laboratory systems* 1987; 2(1-3): 37–52.

[42] Chiachío J, Bochud N, Chiachío M et al. A multilevel bayesian method for ultrasound-based damage identification in composite laminates. *Mechanical Systems and Signal Processing* 2017; 88: 462–477.

[43] Beck JL. Bayesian system identification based on probability logic. *Structural Control and Health Monitoring* 2010; 17(7): 825–847.

[44] Cheung SH and Beck JL. Calculation of posterior probabilities for bayesian model class assessment and averaging from posterior samples based on dynamic system data. *Computer-Aided Civil and Infrastructure Engineering* 2010; 25(5): 304–321.

[45] Chiachío M, Chiachío J, Rus G et al. Predicting fatigue damage in composites: A bayesian framework. *Structural Safety* 2014; 51: 57–68.

[46] Jaynes ET. Information theory and statistical mechanics. *Physical review* 1957; 106(4): 620.

[47] Metropolis N, Rosenbluth AW, Rosenbluth MN et al. Equation of state calculations by fast computing machines. *The journal of chemical physics* 1953; 21(6): 1087–1092.

[48] Hastings WK. Monte carlo sampling methods using markov chains and their applications. *Biometrika* 1970; 57(1): 97–109.

[49] Papadimitriou C. Optimal sensor placement methodology for parametric identification of structural systems. *Journal of sound and vibration* 2004; 278(4-5): 923–947.

[50] Cantero-Chinchilla S, Chiachío J, Chiachío M et al. Optimal sensor configuration for ultrasonic guided-wave inspection based on value of information. *Mechanical Systems and Signal Processing* 2020; 135: 106377.

[51] Suykens JA and Vandewalle J. Least squares support vector machine classifiers. *Neural processing letters* 1999; 9(3): 293–300.

[52] Zapico J, Gonzalez M and Worden K. Damage assessment using neural networks. *Mechanical Systems and Signal Processing* 2003; 17(1): 119–125.

[53] Roberts GO, Rosenthal JS et al. Optimal scaling for various metropolis-hastings algorithms. *Statistical science* 2001; 16(4): 351–367.

[54] Cristianini N, Shawe-Taylor J et al. *An introduction to support vector machines and other kernel-based learning methods*. Cambridge university press, 2000.

[55] Altman NS. An introduction to kernel and nearest-neighbor nonparametric regression. *The American Statistician* 1992; 46(3): 175–185.

[56] McLachlan GJ. *Discriminant analysis and statistical pattern recognition*, volume 544. John Wiley & Sons, 2004.

[57] Breiman L, Friedman J, Stone CJ et al. *Classification and regression trees*. CRC press, 1984.

[58] Gardner P, Liu X and Worden K. On the application of domain adaptation in structural health monitoring. *Mechanical Systems and Signal Processing* 2020; 138: 106550.

[59] Saltelli A, Ratto M, Andres T et al. *Global sensitivity analysis: the primer*. John Wiley & Sons, 2008.

[60] Patelli E, Pradlwarter HJ and Schuëller GI. Global sensitivity of structural variability by random sampling. *Computer Physics Communications* 2010; 181(12): 2072–2081.

[61] Saltelli A. Making best use of model evaluations to compute sensitivity indices. *Computer physics communications* 2002; 145(2): 280–297.

[62] Fang KT, Lin DK, Winker P et al. Uniform design: theory and application. *Technometrics* 2000; 42(3): 237–248.